Extensional deformation of Newtonian liquid bridges

S. Gaudet, G. H. McKinley, and H. A. Stone
Division of Engineering & Applied Sciences, Harvard University, Cambridge, Massachusetts 02138

(Received 31 August 1995; accepted 7 June 1996)

A numerical investigation is presented of axisymmetric, static and elongating, viscous Newtonian liquid bridges confined between identical circular disks. The time-dependent interface shapes and applied forces on the end plates, which separate at a constant prescribed velocity, are calculated as functions of the capillary number, the viscosity ratio between the inner and outer fluids, and an initial bridge configuration characterized by the aspect ratio. The numerical simulations are in excellent agreement with available experimental data and provide useful insight into the different dynamical responses of extending liquid bridge configurations. In particular, liquid bridges surrounded by fluids of a relatively small viscosity deform in a fore-aft symmetrical manner and undergo breakup sooner than in the case of relatively viscous outer fluids, which also require a greater applied force on the end plates to maintain the desired motion. Decreasing the capillary number (increasing interfacial tension) and the initial aspect ratio result in shorter bridge lengths prior to breakup and an increase in the applied forces on the end plates. © *1996 American Institute of Physics.* [S1070-6631(96)02110-1]

I. INTRODUCTION

A mass of liquid connecting a pair of solid surfaces is called a *liquid bridge* (see Figs. 1 and 2). Such a configuration occurs in many natural as well as industrial applications. Examples of these include oil recovery, float-zone crystal growth, powder granulation, flow in porous media, materials processing and the liquid film at the base of the feet of aphids[1] and tree frogs.[2] In enhanced oil recovery applications, for example, there is interest not only in static stability but also in the dynamic evolution of the liquid bridges of viscous crude oil that exist in the interstitial voids of the reservoir as the less viscous displacing fluid is pumped into the reservoir.

The liquid bridge configuration has also been used in rheological studies for experimentally determining the extensional viscosity of non-Newtonian fluids.[3,4] Indeed, such studies motivated our investigation of liquid bridges. Extensional deformations of non-Newtonian fluids are significant in fiber-spinning and extrusion and also can have significant influences on stability and breakup of jets and threads. The extensional viscosity characterizes a fluid's resistance to elongational (or extensional) deformation and for non-Newtonian fluids is a fundamental material property which cannot be inferred from viscometric shearing motions.[5] In many experimental configurations, a column of test fluid is placed between two rigid circular disks which are then separated at a prescribed rate.[6] The tensile forces which are measured on the disks are used to determine the coefficient of tensile resistance to elongational deformation. It is well known that in a homogeneous, steady, uniaxial extensional motion, Newtonian fluids, such as water or syrup, exhibit an extensional or Trouton[7] viscosity that is exactly three times the value of their Newtonian shear viscosity μ. For macromolecular fluids, such as polymer melts, liquid crystals, or DNA solutions, molecular models predict that the extensional viscosity is dependent on the imposed deformation rate and can be 10^2 to 10^5 times larger than the shear-rate-dependent viscosity of the fluid. In this paper we first discuss some static features of liquid bridges and then describe in detail the results of a numerical study of the dynamics of stretching Newtonian liquid bridges. The dynamics of Newtonian liquid bridges is a starting point for ongoing investigations concerning the extensional flow dynamics of non-Newtonian fluids.

Under static conditions, the equilibrium shapes of Newtonian or non-Newtonian liquid bridges confined by rigid surfaces are governed by the Young-Laplace capillarity equation and many studies of the shapes and stability as a function of fluid volume, aspect ratio, end-plate size, gravitational body forces and capillary pressure have been performed.[8–14] Studies of the dynamics, for infinitesimal as well as finite perturbations from a static equilibrium configuration, have focused on liquid bridges confined by circular end plates and depend on three parameters: a Reynolds number, $\rho\sigma R_0/\mu^2$ (the inverse is called the Ohnesorge number) where ρ, μ and σ are, respectively, the density, viscosity and interfacial tension for a liquid bridge with end plates of radius R_0, a Bond number, $\Delta\rho g R_0^2/\sigma$, which measures the importance of gravitational influences, and the viscosity ratio between the inner and outer fluids. Previous investigations include linear and nonlinear stability analyses in the limit of small, or zero, Bond number for low viscosity fluids (Reynolds number $\gg 1$)[15–19] as well as high viscosity fluids.[20] Finite Bond number effects have also been investigated for low viscosity fluids.[21,22] Some of the dynamical investigations include the problem of the breaking of the bridge, rotation of the end plates at the same or different speeds and

 1070-6631/96/8(10)/2568/12/$10.00

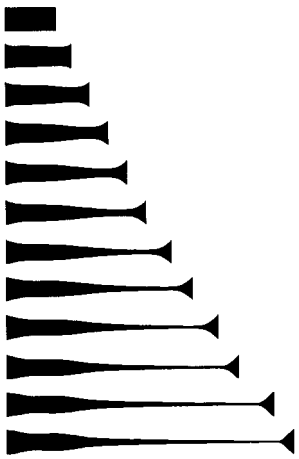

FIG. 1. Simulation of an extending liquid bridge with $\mathscr{C}=1$, $\lambda=1$ and $\Lambda_0=2$. Shapes are shown for the dimensionless times 0.0, 1.1, 2.6, 4.0, 5.4, 6.9, 8.8, 10.7, 12.6, 14.1, 16.9, 18.5. Non-dimensionalization is discussed in Sec. III.

spin-up from rest. An extensive review of this literature is provided by Martinez and Croll.[23] There have also been studies of the influence of the fluid surrounding the liquid column,[19] including viscous oscillations[21] and flow[24,25] in the outer fluid.

However, comparatively little theoretical work has been focused on the extensional dynamics of deforming viscous fluid bridges even for the case of Newtonian fluids. Analytical solutions for extensional motions can be found provided the dynamic shape obtained during deformation is assumed to be identical to the static interface shape corresponding to the instantaneous volume and aspect ratio, which neglects viscous stresses acting on the interface (e.g., see Davis and Frenkel[26]). Alternatively, the liquid column is assumed to remain cylindrical by allowing a moving contact line on the solid surfaces.[26] The extensional deformation of non-Newtonian liquid bridges has been studied experimentally[3,4,27–30] and has also been studied recently using the finite-element method.[31]

Extensional deformations of Newtonian fluids at low Reynolds numbers incorporating motion both inside and outside the fluid column are the main focus of this paper. A sample numerical simulation of a liquid bridge whose right-hand end plate is moved at constant velocity is presented in Fig. 1. We notice the breaking of symmetry about the mid-plane, an effect which depends on the viscosity ratio between the inner and outer fluids, the asymmetric boundary motion and the interfacial tension. It is well known in the liquid bridge literature[13,17,32] that breaking of symmetry can also occur during capillary breakup of static liquid bridges subject to some asymmetric perturbation (e.g., axial acceleration, disks of different diameters). The results in this paper highlight the dynamical role of stretching and viscosity in modifying the long-time evolution of the bridge (see section IV C for further discussion). Fluid flow occurs because of the end-plate motion and additional interfacial-tension-driven motions arise owing to curvature variations; breakup is expected shortly after the final simulation shown. The total applied forces on the end plates are typically measured during liquid bridge stretching experiments and are calculated as functions of time in our simulations. Each of the above topics are discussed in this paper.

We first briefly review in Sec. II the classical results obtained in the static limit, but recast the results in a form relevant to typical experimental configurations. The major part of this paper treats the dynamics of Newtonian liquid bridges undergoing extensional deformations between parallel circular plates. This topic is investigated numerically using a boundary integral method for viscous free-boundary problems. In Sec. III a brief summary of the numerical method is given. In Sec. IV the simulations are compared with available experimental results and we also systematically investigate the effects of interfacial tension, viscosity ratio between the two fluids and the initial aspect ratio of the bridge.

II. STATICS

We begin with a discussion of the static shapes assumed by a liquid bridge, which is a problem studied last century by Plateau.[8] The problem was reconsidered by Erle *et al.*[9] and Gillette and Dyson,[10] and recent microgravity experiments have generated renewed interest in this problem.[13,23] First, we present the equations governing the static equilibrium shapes of liquid bridges and second we present numerical results for equilibrium bridge configurations similar to the stretching experiments described in Sec. IV. Extensive numerical calculations, as well as some experiments, involving the shape and stability of static liquid bridge configurations have been reported in the literature.[13,32]

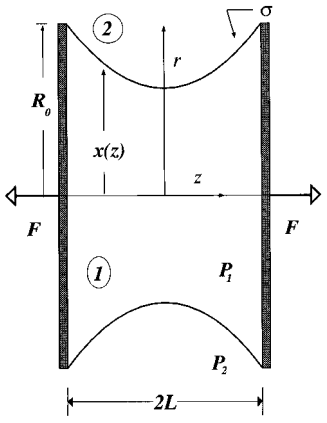

FIG. 2. Axisymmetric liquid bridge geometry under static conditions.

Consider the static axisymmetric liquid bridge shown in Fig. 2, where R_0 and $2L$ denote, respectively, the end-plate radius and bridge length in some equilibrium configuration, and $x(z)$ represents the equilibrium radial position of the interface as a function of the axial coordinate z. The fluids inside and outside the liquid bridge are distinguished by the subscripts 1 and 2, respectively, and the enclosed fluid volume, V, of the liquid bridge is

$$V=\pi\int_{-L}^{L}x^2(z)dz. \tag{1}$$

In order to maintain the bridge in a fixed configuration it is necessary to apply a force of magnitude F on each end plate. For example, when the bridge is in tension the force on the right-hand end plate is positive, $F>0$, and directed along the positive z-axis.

In experiments designed to determine the maximum stable length of a liquid column, the bridge may be deformed quasi-statically from one equilibrium configuration to another. It is convenient to introduce dimensionless measures of the geometric configuration. The aspect ratio is defined as $\Lambda=L/R_0$. The dimensionless volume of the bridge relative to the volume of a right circular cylinder of length $2L$ is $\mathscr{V}=V/2\pi R_0^2 L$. Experiments performed by stretching a bridge of *constant fluid volume V* from one equilibrium length to another thus correspond to maintaining a constant value of $\mathscr{V}\Lambda\equiv V/2\pi R_0^3$.

It is well known that in the case of constant interfacial tension, σ, the equilibrium interface shape, $x(z)$, is the surface of revolution that minimizes the surface area. Gillette and Dyson[10] studied this problem theoretically using the calculus of variations and demonstrated that the Euler-Lagrange equation for the liquid bridge geometry is equivalent to the Young-Laplace equation, which in the absence of gravitational body forces leads to the static force balance,

$$\frac{2\pi\sigma x(z)}{(1+(dx/dz)^2)^{1/2}}-\pi x(z)^2\Delta P=F, \tag{2}$$

where $\Delta P=P_1-P_2$ denotes the static pressure difference between the inner and outer fluids. A dimensionless form of equation (2) can be written as

$$\frac{2\hat{x}(\hat{z})}{(1+(d\hat{x}/d\hat{z})^2)^{1/2}}-\mathscr{P}\hat{x}^2=\mathscr{F}, \tag{3}$$

where all lengths are nondimensionalized by R_0, $\mathscr{P}=\Delta P R_0/\sigma$ is the dimensionless pressure difference and $\mathscr{F}=F/(\pi\sigma R_0)$ is the dimensionless force acting on either of the end plates.

For $\mathscr{P}=0$ there is no volume constraint and the problem is equivalent to the classical soap film problem whose solution yields a catenary[9] given by the equation

$$\hat{x}(\hat{z})=c_1\cosh\left(\frac{\hat{z}}{c_1}\right). \tag{4}$$

The constant c_1 is chosen to satisfy the boundary condition $\hat{x}(\Lambda)=1$.

In cases where $\mathscr{P}\neq 0$, equation (3) can be solved analytically in parametric form. The interface shape and the liquid bridge volume are expressed in terms of elliptic integrals as functions of the dimensionless pressure difference $\mathscr{P}$, applied force $\mathscr{F}$ and the aspect ratio Λ.[10] For identical end-plate sizes the equilibrium shapes obtained have the symmetry $\hat{x}(\hat{z})=\hat{x}(-\hat{z})$.

Since the static equilibrium configuration represents the limiting case of vanishing end-plate velocities for the extending, constant volume liquid bridges studied in Sec. IV, it is natural to calculate the static bridge shapes given an aspect ratio Λ and a fixed fluid volume $\mathscr{V}\Lambda$. This procedure of setting the bridge volume and the geometric configuration is one which would also be most common in a laboratory experiment. Because the parametric equations[10] give the interface shape and volume as functions of the pressure difference, the applied force, and constant parameters determined by setting the geometric dimensions (aspect ratio and length or diameter), a numerical approach is required. In particular, we obtained numerical results by using an iterative scheme in which the dimensionless volume $\mathscr{V}$, and the aspect ratio Λ, as well as the plate diameter, were fixed and the parametric equations given by Gillette and Dyson[10] and the constraint (1) were solved for $\mathscr{P}$, $\mathscr{F}$ and the interface shape. We note that this procedure is different than that used by Gillette and Dyson who specified $\mathscr{P}$ and $\mathscr{F}$ and so determined the interface shape and fluid volume required in an explicit manner using the parametric equations they had derived. Our procedure, i.e., specifying $\mathscr{V}$ and Λ, is similar in spirit to the approach utilized by Meseguer and Sanz,[17] who solved a boundary value problem numerically to obtain the equilibrium shapes. The results from these two different numerical implementations are the same although they are presented in different manners.

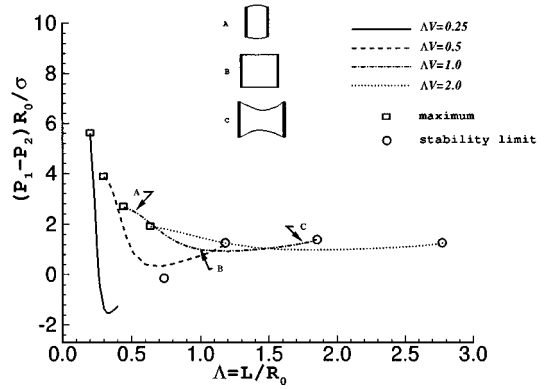

FIG. 3. Nondimensional pressure difference $\mathscr{P}$ versus aspect ratio Λ for various fixed fluid volumes, $\Lambda\mathscr{V}$. The letters indicate the interface shapes at the conditions identified by the arrows. Circles denote the largest aspect ratio for which a stable shape exists (Ref. 10); rectangles denote a pressure maximum and for smaller aspect ratios the iterative numerical scheme utilized here fails.

In Figs. 3 and 4 we present the dimensionless pressure

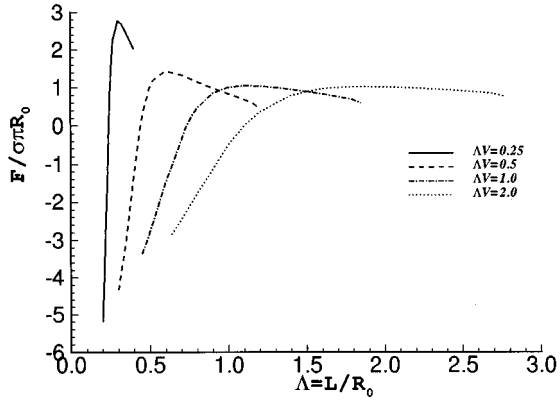

FIG. 4. Nondimensional applied force $\mathscr{F}$ versus aspect ratio Λ for various fixed fluid volumes, $\Lambda\mathscr{V}$.

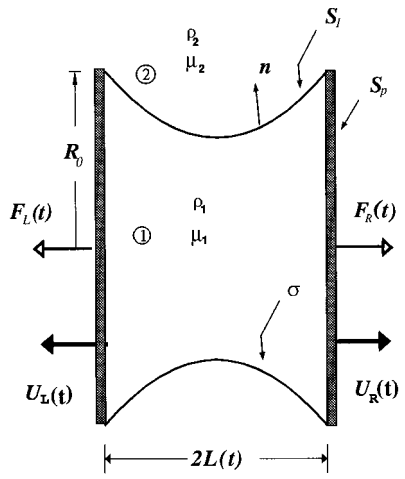

FIG. 5. Newtonian liquid bridge undergoing steady stretching. For all the calculations in this paper we take $U_L=0$.

difference and the applied force on the end plates as a function of the aspect ratio and the different values of the fluid volume. Conditions for each curve were chosen so that the dimensionless fluid volume is $\mathscr{V}=1$ at initial aspect ratios of $\Lambda=0.25,0.5,1$ and 2, respectively. The dimensionless pressure difference and force at these conditions are $\mathscr{P}=1$ and $\mathscr{F}=1$. Representative shapes for concave and convex liquid bridges are also shown in Fig. 3. We first note that in Fig. 3, the pressure difference is negative for the case $\Lambda\mathscr{V}=0.25$ for aspect ratios $\Lambda>0.25$. For a concave liquid bridge with these parameters, the interface curvature is such that at a given point on the interface the pressure difference must be negative in order to balance the outward directed resultant force produced by interfacial tension. For all the other cases presented in Fig. 3, the interfacial tension force on an element of the interface is directed towards the inner fluid.

We have also indicated on Fig. 3 circles which denote the static stability limit for the given volume of fluid beyond which no equilibrium shapes exist (Figs. 6 and 7 of Ref. 10). Rectangles indicate the point at which the maximum pressure difference occurs. We note from Fig. 4 that for constricted bridges a tensile force, $\mathscr{F}>0$, is always required, whereas for sufficiently outwardly bulging (convex) bridges a negative force, $\mathscr{F}<0$, is required to maintain a constant plate separation. This variation in the sign of the force may also be verified by considering equation (3).

We next turn to a detailed consideration of the dynamical problem in which the end plates are separated as a function of time. Henceforth we also cease to denote explicitly dimensionless variables with a caret.

III. BOUNDARY INTEGRAL FORMULATION

A theoretical study of the dynamical evolution of a deforming liquid bridge is difficult owing to the free-boundary character of the problem: the location of the fluid-fluid interface, on which boundary conditions are to be applied, must be determined as part of the solution. Here we focus on viscously dominated, low Reynolds number motion of liquid bridges. For this limit, the boundary integral method is an efficient and well-established numerical solution technique.[33–35] The viscous dynamics of stretching bridges studied here may be contrasted with investigations of liquid bridges based on an inviscid irrotational flow approximation.[17,19]

We consider the elongation of a Newtonian liquid bridge schematically indicated in Fig. 5. Properties of the bridge fluid are again denoted with a subscript 1 and those of the surrounding fluid are denoted by 2. The external fluid is treated as unbounded so that the fluid has two internal boundaries, the fluid-fluid interface S_I and the end-plate surfaces S_P. We will restrict ourselves to axisymmetric bridge shapes so that the end-plate surfaces are assumed to have an axisymmetric shape and, in particular, we focus attention on the case of thin flat (circular disk) surfaces shown in Fig. 5, though other axisymmetric-shaped end plates, e.g., cones, have been numerically simulated and are often used in the laboratory. For all the calculations shown in this paper, the right end plate is moved with constant velocity $U_R(t)=U$ and the left end plate remains stationary ($U_L=0$). Consequently, the aspect ratio Λ increases linearly with time, while the product $\Lambda\mathscr{V}$, corresponding to the volume of the bridge, remains constant. Interfacial shapes in this simple bridge configuration may be compared directly with experimental data, available in the literature[28] and generated in our laboratory.[30] The analysis given below may also be generalized to the case where each end plate moves with an arbitrary prescribed velocity.

A. Integral representation of low Reynolds number fluid motions

Fluid flows for which the Reynolds number $\mathscr{R}=\rho UR_0/\mu$ is small, so that the inertia terms in the Navier-Stokes equations can be neglected, are governed by the linear (quasi-steady) Stokes equations and the continuity equation. For incompressible flow of a fluid with viscosity μ_i and density ρ_i, the velocity $\mathbf{u}$ and pressure P satisfy ($i=1,2$)

$$\nabla\cdot\mathbf{T}_i=-\nabla P_i+\mu_i\nabla^2\mathbf{u}_i+\rho_i\mathbf{g}=\mathbf{0}, \tag{5}$$

$$\nabla\cdot\mathbf{u}_i=0,$$

where the Newtonian stress tensor $\mathbf{T}$ has been defined to incorporate the hydrostatic pressure,

$$\mathbf{T}=-(P-\rho\mathbf{g}\cdot\mathbf{x})\mathbf{I}+\mu(\nabla\mathbf{u}+(\nabla\mathbf{u})^T), \tag{6}$$

$\mathbf{g}$ denotes the gravitational acceleration and $\mathbf{x}$ denotes the position vector. The velocity is continuous across all interfaces and the stress jump boundary condition at the deforming fluid-fluid interface is

$$\mathbf{n}\cdot\mathbf{T_2}-\mathbf{n}\cdot\mathbf{T_1}=\sigma(\nabla_s\cdot\mathbf{n})\mathbf{n}-\Delta\rho(\mathbf{g}\cdot\mathbf{x})\mathbf{n},\quad \mathbf{x}_s\in S_I, \tag{7}$$

where $\mathbf{n}$ is the unit normal directed into fluid 2, $\nabla_s=(\mathbf{I}-\mathbf{nn})\cdot\nabla$ is the gradient operator along the interface, $\nabla_s\cdot\mathbf{n}$ is the mean interface curvature, the interfacial tension σ is assumed constant and $\Delta\rho=\rho_1-\rho_2$.

The derivation of an integral equation representation for the solution of this boundary value problem is straightforward.[33–35] The solution of the integral equation, defined over the bounding surfaces S_P and S_I, yields the

force distribution on the end plates and the interfacial velocities, from which the shape of the liquid bridge can be determined as a function of time. The integral equation representation of the solution is (assuming the velocity vanishes far away)

$$-\frac{1}{\mu_2}\int_{S_I+S_P}[\mathbf{n}\cdot\mathbf{T}_2-\mathbf{n}\cdot\mathbf{T}_1]\cdot\mathbf{J}(\mathbf{x}|\mathbf{y})dS_y+(\lambda-1)\times\int_{S_I+S_P}\mathbf{n}\cdot\mathbf{K}(\mathbf{x}|\mathbf{y})\cdot\mathbf{u}\,dS_y=\begin{cases}\lambda\mathbf{u}_1(\mathbf{x}), & \mathbf{x}\in V_1,\\ \frac{1}{2}(1+\lambda)\mathbf{u}_1(\mathbf{x}_s), & \mathbf{x}_s\in S_I+S_P,\\ \mathbf{u}_2(\mathbf{x}), & \mathbf{x}\in V_2,\end{cases}\tag{8}$$

where $\lambda=\mu_1/\mu_2$ is the viscosity ratio, $\mathbf{y}$ is the integration variable and the tensors $\mathbf{J}$ and $\mathbf{K}$ are

$$\mathbf{J}(\mathbf{x}|\mathbf{y})=\frac{1}{8\pi}\left(\frac{\mathbf{I}}{r}+\frac{\mathbf{rr}}{r^3}\right),\qquad \mathbf{K}(\mathbf{x}|\mathbf{y})=-\frac{3}{4\pi}\frac{\mathbf{rrr}}{r^5},\quad \text{with } \mathbf{r}=\mathbf{x}-\mathbf{y};\quad r=|\mathbf{r}|.\tag{9}$$

The integral equation may be nondimensionalized by choosing U, R_0 and $\mu_1 U/R_0$, respectively, as the characteristic velocity, length and stress. By using the stress jump at the fluid-fluid interface (7), equation (8) is expressed in dimensionless form as

$$-\frac{1}{\mathscr{C}}\int_{S_I}[\mathbf{n}(\nabla_s\cdot\mathbf{n})-\mathscr{B}(\mathbf{e}_g\cdot\mathbf{y})\mathbf{n}]\cdot\mathbf{J}(\mathbf{x}|\mathbf{y})dS_y+\left(1-\frac{1}{\lambda}\right)\int_{S_I+S_P}\mathbf{n}\cdot\mathbf{K}(\mathbf{x}|\mathbf{y})\cdot\mathbf{u}dS_y-\int_{S_P}\mathbf{f}\cdot\mathbf{J}(\mathbf{x}|\mathbf{y})dS_y=\begin{cases}\mathbf{u}_1(\mathbf{x}), & \mathbf{x}\in V_1,\\ \frac{1}{2}\left(1+\frac{1}{\lambda}\right)\mathbf{u}_1(\mathbf{x}_s), & \mathbf{x}_s\in S_I+S_P,\\ \frac{1}{\lambda}\mathbf{u}_2(\mathbf{x}), & \mathbf{x}\in V_2,\end{cases}\tag{10}$$

where $\mathbf{e}_g$ is a unit vector in the direction of gravity. We have introduced two dimensionless parameters, the capillary number $\mathscr{C}$ and the Bond number $\mathscr{B}$,

$$\mathscr{C}=\frac{\mu_1 U}{\sigma},\qquad \mathscr{B}=\frac{\Delta\rho g {R_0}^2}{\sigma},\tag{11}$$

which represent, respectively, the relative magnitudes of viscous and gravitational body forces to interfacial tension forces. In order to preserve the axisymmetry in the problem, we must have $\mathbf{e}_g\|\mathbf{e}_z$. Also, the $\mathbf{J}$ integral has been subdivided into integrals over the deforming interface S_I and the end-plate surfaces S_P, and the stress jump across the rigid end plates is denoted as $\mathbf{f}=\mathbf{n}\cdot\mathbf{T}_2-\mathbf{n}\cdot\mathbf{T}_1$ on S_P.

Equations (10), for $\mathbf{x}_s\in S_P$ and $\mathbf{x}_s\in S_I$, represent coupled integral equations of the second kind for the unknown interfacial velocity $\mathbf{u}(\mathbf{x}_s\in S_I)$ and the end-plate stress jump $\mathbf{f}(\mathbf{x}_s\in S_P)$. Boundary conditions are specified on the end plates where the velocities are $\mathbf{u}(\mathbf{x}_s\in S_P)=\mathbf{0}$ on the left end plate and $\mathbf{u}(\mathbf{x}_s\in S_P)=\mathbf{e}_z$ on the right end plate. Specification of an initial surface configuration completes the problem statement. For all the cases presented in this paper the initial interface shape was that of a circular cylinder at an initial aspect ratio Λ_0.

The total force required to keep the left end plate stationary is always negative and is obtained by adding the static (interfacial tension) contribution to the integrated dynamic (viscous and pressure) contributions on the plate. A force balance on the left end plate thus yields the dimensionless equation

$$\mathscr{F}_L=\frac{F_L}{\mu_1 U R_0}=\int_{S_P}\mathbf{n}\cdot[\mathbf{n}\cdot\mathbf{T}_2-\mathbf{n}\cdot\mathbf{T}_1]dS-\frac{2\pi}{\mathscr{C}(1+(\partial x/\partial z)^2)^{1/2}}.\tag{12}$$

This definition differs from that used in the static simulations reported in Sec. II.

B. Discretization of the bounding surfaces

Since the geometry is assumed to be axisymmetric, the azimuthal integration in equation (10) can be performed analytically rendering all surface integrals to line integrals along the axial coordinate.[36] The bounding surfaces S_I and S_P are subdivided, respectively, into N_I and N_P elements over which the unknown velocities and stress jumps are assumed constant. The nodal points where unknowns are evaluated are defined at the middle of the surface elements.

At a given time step, a $2(N_I+2N_P)\times 2(N_I+2N_P)$ system of linear equations is obtained by writing the discretized version of equation (10) for the N_I points on the interface S_I and the $2N_P$ points on the two end plates S_P. The resulting system of equations is solved using standard linear system solvers and, with the computed velocities, an explicit Euler time integration is used to update the interface shape according to the kinematic condition tracking the interface following the normal component of motion,

$$\frac{d\mathbf{x}_s(t)}{dt}=(\mathbf{u}(t)\cdot\mathbf{n})\mathbf{n},\quad \text{for } \mathbf{x}_s\in S_I.\tag{13}$$

Here time has been nondimensionalized with the convective time scale R_0/U.

The interface shape is approximated by a cubic spline interpolant with which second derivatives are evaluated in order to obtain the surface curvature.[37] Typically we choose $N_I=41$ and $N_P=15$. In the results reported here, gravitational body forces are neglected, i.e., $\mathscr{B}=0$; it is nevertheless straightforward to solve (10) for axisymmetric geometries with $\mathscr{B}\neq 0$. Numerical convergence checks have been performed to ensure convergence with time step as well as with spatial discretization.

IV. NUMERICAL RESULTS

In this section we present results of numerical simulations of the stretching of Newtonian liquid bridges, an example of which has been shown above in Fig. 1. Before

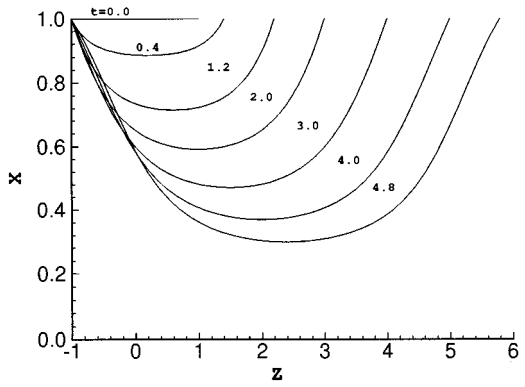

FIG. 6. Interface evolution during steady stretching. The left plate is held fixed and the right plate is moved at unit speed. $\mathscr{C} = 1$; $\lambda = 3000$; $\Lambda_0 = 1$. Dimensionless times for each of the interfacial shapes are indicated.

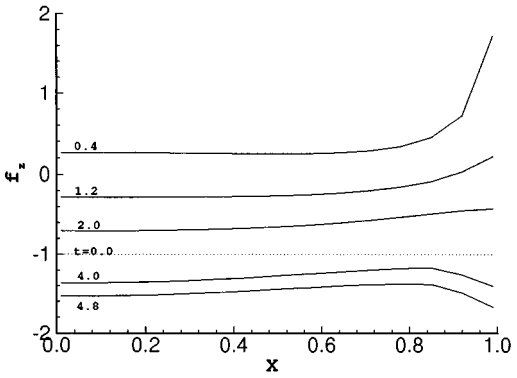

FIG. 7. Distribution of the normal stress jump $f_z = \mathbf{e}_z \cdot \mathbf{f}$ on the left end plate for the same conditions as Fig. 6.

presenting any detailed results, we discuss an order of magnitude description of the expected flows. At a given point on the interface, if interfacial tension and local curvature are such that interfacial tension forces dominate viscous forces, $\mathscr{C} = \mu_1 U/\sigma \ll 1$, the local normal velocity has magnitude $\sigma/[\mu(1+1/\lambda)]$. However, in a situation where the reverse is true, $\mathscr{C} = \mu_1 U/\sigma \gg 1$, the interface shape is such that motion conforms with stretching of a family of cylinders and the normal component of velocity has magnitude U/Λ.

Similarly, by use of (12), we arrive at an order-of-magnitude scaling for the dimensionless applied force on the left end plate:

$$\mathscr{F}_L \approx O\left(\frac{\pi}{\mathscr{C}(1+(\partial x/\partial z)^2)^{1/2}} + \frac{1}{\Lambda^2}\left(1+\frac{1}{\lambda}\right)\right), \tag{14}$$

where $\partial x/\partial z$ represents the slope of the interface at the left end plate. The first term accounts for interfacial tension or capillary forces while the second represents the viscous contribution to the total force. A very extended liquid bridge tends to require smaller forces to maintain the left end plate in a fixed position because of its relatively large aspect ratio, Λ, and hence there is a smaller contribution to $\mathscr{F}_L$ from viscous stresses. For early times, viscous effects attain their largest values and can be larger than capillary effects for small enough aspect ratios. Finally, large interfacial tensions always lead to greater applied forces and we further note that the outer fluid may greatly increase the required force for $\lambda < 1$ because of the added viscous dissipation in the external fluid.

We begin our study of dynamics with a simulation for a relatively large viscosity ratio, $\lambda = 3000$, since large viscosity ratios are typical of most liquid bridge stretching experiments.[3,4,30] We then consider in turn the effect of varying $\mathscr{C}$, λ and the initial aspect ratio, Λ_0. In all cases reported here we take $\mathscr{B} = 0$.

A. An example of stretching a very viscous thread

In Fig. 6 we present a sequence of interface shapes for an elongating liquid bridge with $\lambda = 3000$ and $\mathscr{C} = 1$. The bridge is initially at rest with an aspect ratio $\Lambda_0 = 1$ and is stretched with a constant unit velocity to a final aspect ratio $\Lambda = 3.4$. The fluid filament thins as the stretching progresses. Under static conditions a liquid bridge with this final aspect ratio is unstable, though here the bridge remains intact as long as stretching occurs. Also, we observe that in the absence of gravitational body forces and inertia, for large viscosity ratios λ, and for this value of the capillary number $\mathscr{C} = 1$, the minimum interfacial radius occurs at the midpoint of the fluid column and the bridge is fore-aft symmetric. We will see in Sec. IV D that this type of symmetrical deformation only occurs in situations where, for a finite capillary number, the outer fluid is significantly less viscous than the inner one.

In Fig. 7 we show the evolution of the axial component of the normal stress jump $\mathbf{e}_z \cdot \mathbf{f}$ acting along the left end plate for the deforming bridge shown in Fig. 6. The stress distribution is nearly uniform across the plate except near the contact line ($x > 0.8$) at the rim where the velocity gradients are initially larger. At early times, viscous stresses due to elongation of the bridge are largest and the dynamic contribution to the axial force is positive, i.e., the viscous traction attempts to drag the left end plate in the positive z-direction. The viscous contribution to the dynamic force is proportional to the product of the viscosity μ_1 and the extension rate U/L so that as the bridge elongates at constant velocity the viscous contribution decreases in importance and the capillary pressure eventually dominates leading to a negative value of $f_z = \mathbf{e}_z \cdot \mathbf{f}$. To further illustrate this point vector plots of the velocity field inside the extending liquid bridge are presented in Fig. 8, which show that the viscous contribution to the applied force can eventually change sign because of a flow reversal near the left end plate (Fig. 8c). The accelerated pinching of the high curvature regions leads to a net flow in the negative z-direction near the left end plate. As a consequence of this change in flow direction bulging occurs near the end plates. We will see later that bulging only occurs for certain values of $\mathscr{C}$, λ and Λ_0.

In Fig. 9 we present a comparison of the evolution of the total tensile force $\mathscr{F}_L$ on the fixed left end plate as a function of time for $\mathscr{C} = 0.1, 1, 10$. The liquid bridge in each case was stretched to a final aspect ratio $\Lambda = 1.5$ at $t = 1$ and subsequently both end plates were held in fixed positions while the interface was allowed to deform further until it attained a

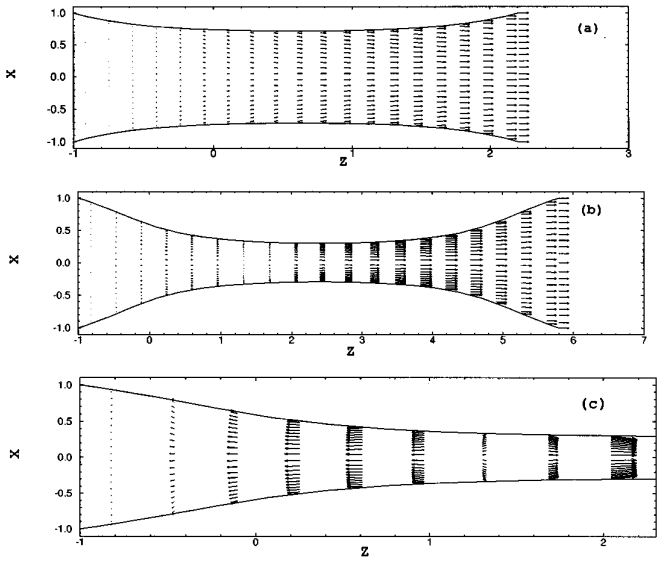

FIG. 8. Velocity fields inside an extending liquid bridge at different dimensionless times. $\mathscr{C}=1$, $\lambda=3000$ and $\Lambda_0=1$. (a) $t=1.2$; (b) $t=4.8$, (c) $t=4.8$. The absolute length of the velocity vectors in (c) have been magnified by a factor of 7.

stable static shape ($\Lambda=1.5$ is within the static stability boundary for this bridge volume). As the bridge elongates, the tensile force decreases monotonically, except for a short initial transient. Each of the final static shapes is in good agreement with results obtained from the static analysis of Sec. II. Upon cessation of stretching, the bridges rapidly attain the equilibrium static configuration whose end-plate forces are shown by the horizontal dashed lines. The open symbols indicate the values of the dimensionless forces initially required to maintain the static cylindrical equilibrium shapes. Different dimensionless values of the static force arise here because of the viscous scaling of the stresses; for a cylindrical liquid bridge in static equilibrium the dimensional force is $F_L=-\pi\sigma R_0$, regardless of the aspect ratio, and so $\mathscr{F}_L=-\pi/\mathscr{C}$.

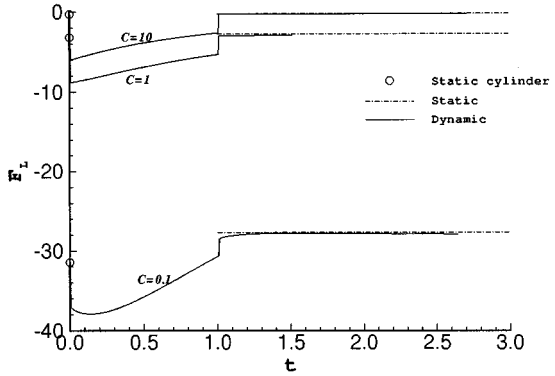

FIG. 9. Evolution of the total dimensionless tensile force $\mathscr{F}_L$ on the left end plate. At dimensionless time $t=1$ the right plate is brought to rest and the bridge evolves to the theoretical static shape (horizontal dashed line); $\lambda=3000$, $\Lambda_0=1$. The open symbols ''o'' indicate the dimensionless force required to maintain a cylindrical liquid bridge in static equilibrium.

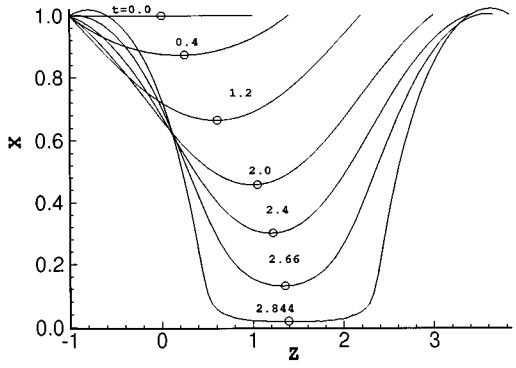

FIG. 10. Evolution of a viscous liquid bridge; $\lambda=3000$, $\mathscr{C}=0.115$, $\Lambda_0=1$. The numerical simulation is continued almost to the point of breakup.

B. Comparison with experimental results

The numerical simulations of liquid bridge dynamics may be compared directly with available experimental data. Kröger *et al.*[28] performed stretching experiments in a neutral buoyancy tank and measured the evolving bridge shape. We select their experiment performed at 1 mm/s in a Newtonian fluid-fluid system with viscosity ratio $\lambda=3000$ and $\mathscr{C}=0.115$ for which the Reynolds number is sufficiently small ($\mathscr{R}=\rho_1 U R_0/\mu_1\approx 0.03$) to enable comparison with our numerical simulations. Figure 10 presents the sequence of interface shapes obtained numerically for these conditions. At long times the middle of the filament thins rapidly and the fluid near the end plates bulges outwards, which is indicative of a reverse flow near the end plates (similar to that shown in Fig. 8) and the incipient breakup of the bridge into two hemispherical blobs and satellite drops.

A direct comparison of the numerical and experimental results is presented in Fig. 11, where the minimum filament radius x_{mid} is shown as a function of time. The results are in good agreement even though the experiment is performed at a small but finite Reynolds number.

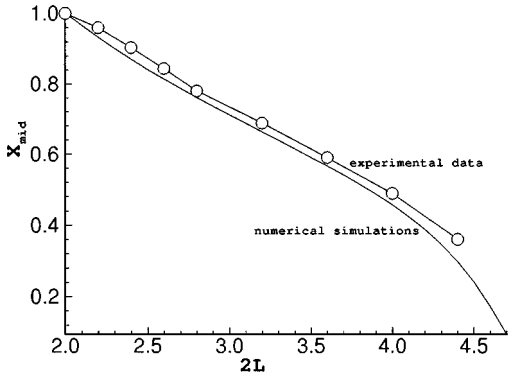

FIG. 11. A comparison of the experimental results of Kröger *et al.* (Ref. 28) with the minimum filament radius calculated numerically for the same conditions as Fig. 10.

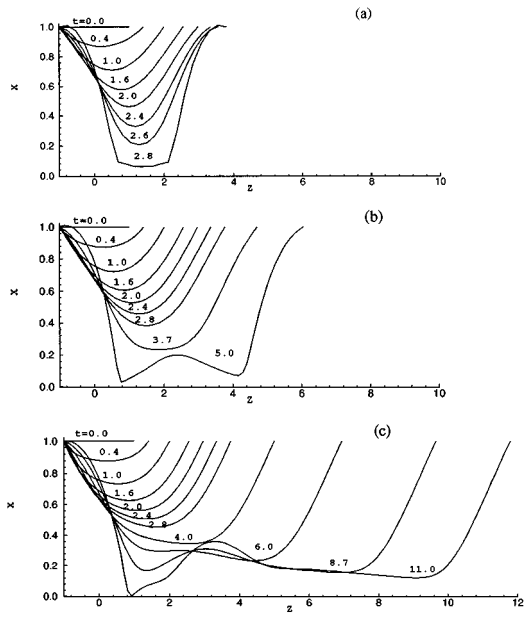

FIG. 12. The effect of the viscosity ratio $\lambda=\mu_1/\mu_2$ on the evolution of the fluid interface; $\mathscr{C}=0.1$, $\Lambda_0=1$, $\mathscr{B}=0$. (a) $\lambda=100$, (b) $\lambda=0.5$, (c) $\lambda=0.1$.

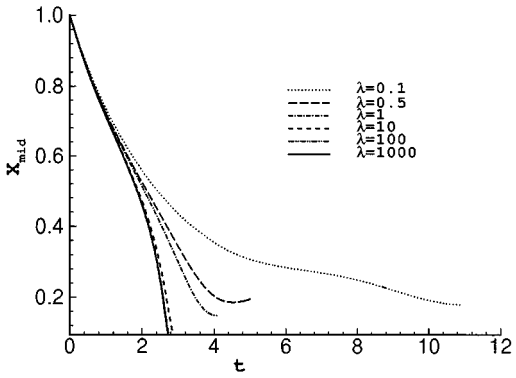

FIG. 13. The effect of λ on the evolution of the liquid bridge mid-point radius; $\mathscr{C}=0.1$, $\Lambda_0=1$, $\mathscr{B}=0$. The curves for $\lambda=100$ and $\lambda=1000$ nearly superpose.

C. Effect of viscosity ratio

In this section we present results for the effects of the viscosity ratio λ on the dynamics of extending Newtonian liquid bridges. These calculations are of importance in understanding experimental observations of deforming liquid bridges in Plateau tanks[19,30] since the viscosity of the external density-matching fluid may play an important role in the observed dynamics. Again the left end plate is fixed and the right plate translates at unit speed and as we now show the asymmetric boundary condition results in asymmetric interface distortions for a range of viscosity ratios. In Fig. 12, interface shapes are shown for an extending liquid bridge with $\mathscr{C}=0.1$, an initial aspect ratio $\Lambda_0=1$, and viscosity ratios $\lambda=0.1,0.5,100$. As the outer fluid viscosity increases (λ decreases), breakup occurs at increasingly greater liquid bridge lengths and the shapes lose the fore-aft symmetry observed at high values of λ. On the other hand, for $\lambda\geqslant 100$, the outer fluid has little dynamical influence and for the small capillary number calculations shown, the middle of the fluid column thins increasingly rapidly as the local curvature increases. Simultaneously, bulging of the bridge occurs near the end plates as a result of the flow reversal discussed and shown above. Significantly less bulging near the right end plate occurs for smaller values of λ, which is a direct consequence of the increase in the outer fluid viscosity and an increased resistance to deformation.

It is worth noting that liquid bridges tend to deform in a symmetrical manner (fore-aft symmetry) when the outer fluid viscosity is small compared to the inner fluid viscosity. In the case where $\mathscr{C}=0.1$, the numerical results indicate such symmetric deformations occur for $\lambda\geqslant 100$ during the entire time of the simulations. For cases in which interfacial tension plays a less significant role [$\mathscr{C}>O(1)$], symmetrical deformations for the imposed asymmetric boundary conditions occur for somewhat higher viscosity ratios; i.e., as the magnitude of interfacial tension stresses decreases, motion of the outer fluid can influence the dynamics enough to break the symmetry even for $\lambda>100$. Nevertheless, any asymmetries which occur during deformation are accentuated as breakup occurs. For large interfacial deformations, the spatial discretization of the mesh becomes apparent as sharp curves appear in regions of high curvatures. In the simulations, however, the shape is smooth since a cubic spline is used to represent the interface.

It is worth contrasting the breaking of fore-aft symmetry observed here with the well-known symmetry breaking documented for static liquid bridges.[13,17,32] For a static bridge bound by equal disks there is a minimum dimensionless fluid volume below which a bridge is unstable for a given aspect ratio. This result is commonly represented as a curve in a minimum volume versus aspect ratio plot (e.g., Gillette and Dyson). Analyses based upon the Young-Laplace equation,[14] including gravitational effects, have shown that static liquid bridges with $\Lambda>\Lambda_c$ lose fore-aft symmetry as they undergo capillary breakup, whereas for $\Lambda<\Lambda_c$ the fore-aft symmetry is retained; Λ_c denotes a critical aspect ratio. These stability results are in agreement with experiments[32] and inviscid calculations[17] that follow the evolution of a static interface responding to a given perturbation. For the case of no gravitational effects, the critical aspect ratio has the value $\Lambda_c=2.13$; the corresponding minimum dimensionless volume is $\mathscr{V}_c=0.57$ and this also corresponds to an initially cylindrical liquid bridge of aspect ratio $\Lambda_0\approx 1.2$ that has been stretched quasi-statically to its minimum stable configuration. However, dynamical effects owing to the presence of viscous stresses from the inner and outer fluids alter the dynamical evolution of the bridge. In particular, it is possible to start with an initially cylindrical liquid bridge with aspect ratio $\Lambda_0>1.2$ which evolves with fore-aft symmetric shapes at all future times in our simulations. For example, a calculation (not shown here) pulling a bridge at both end plates with $\Lambda_0=2$, $\mathscr{C}=0.1$ and $\lambda=0.1$ evolves symmetrically, even up to $\Lambda(t)=10$, in a manner similar to that shown in Fig. 12b even though static bridges undergo asymmetric capillary breakup for values of the as-

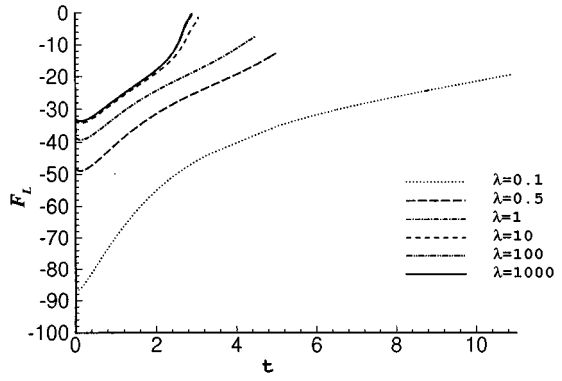

FIG. 14. The effect of λ on the evolution of applied force on the left end plate; $\mathscr{C}=0.1$, $\Lambda_0=1$, $\mathscr{B}=0$. The curves for $\lambda=100$ and $\lambda=1000$ nearly superpose.

pect ratio $\Lambda>\Lambda_c=2.13$. By contrast for a simulation with $\Lambda_0=1$, $\mathscr{C}=10^8$, $\lambda=0.1$ asymmetries are visibly apparent for $\Lambda(t)\approx 1.5<\Lambda_c$. These deviations from static and inviscid predictions are due to viscous effects and are discussed in more detail in Sections IV D and IV E.

The evolution of the mid-point radius of the interface and the dimensionless applied force on the left end plate are presented in Figs. 13 and 14 for $0.1\leqslant\lambda\leqslant 10^3$, $\mathscr{C}=0.1$ and $\Lambda_0=1$. These plots again illustrate that the outer fluid no longer influences the qualitative dynamics of deformation for values of $\lambda\geqslant 100$. In fact, the curves for $\lambda\geqslant 10$ are nearly indistinguishable. We also note that for large λ the initial force is $\mathscr{F}_L\simeq-\pi/\mathscr{C}$ while the dependence of the initial force on λ approximately scales as $(1+1/\lambda)$, which are the two features present in the scaling expression for the dimensionless applied force at early times given in equation (14).

As was suggested in the previous section and can be observed in Fig. 14, significantly more work can be required to elongate the fluid column when the outer fluid has nonnegligible viscosity because of the increased viscous dissipation outside the fluid bridge. We notice that as breakup of the thread occurs, then in the case of large values of λ the applied force on the stationary end plate vanishes since after breakup no external forces act upon the plate (which now has a hemispherical blob of fluid attached to it). However, in cases where λ is $O(1)$ or smaller, there is fluid motion in the outer viscous fluid prior to breakup and so a certain amount of force is still required to maintain the left-hand end plate stationary.

D. Effect of capillary number

In experimental configurations designed to determine the Trouton or extensional viscosity of viscous Newtonian or non-Newtonian liquids, initially cylindrical fluid filaments are deformed at a range of extension rates and the resulting tensile force measurements are used to calculate the extensional viscosity. In the analysis of results from such experiments, surface tension is either assumed to be negligible or the fluid filament is taken to be cylindrical at all times. In this section we report results for the effects of the capillary number $\mathscr{C}$ on the dynamics of extending Newtonian liquid bridges.

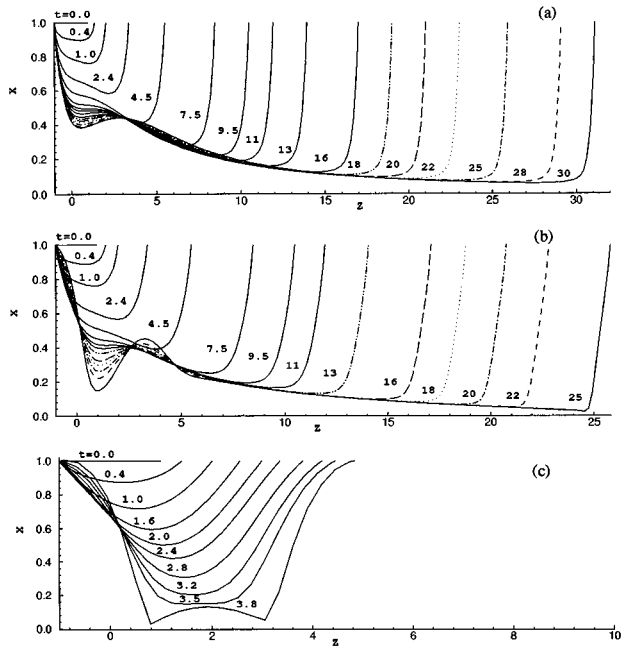

FIG. 15. The effect of $\mathscr{C}$ on the evolution of the fluid interface; $\lambda=1$, $\Lambda_0=1$, $\mathscr{B}=0$. (a) $\mathscr{C}=10$, (b) $\mathscr{C}=1$, (c) $\mathscr{C}=0.1$.

In Fig. 15 interface shapes for $\lambda=1$, initial aspect ratio $\Lambda_0=1$ and $\mathscr{C}=0.1,1,10$ are presented. At lower plate velocities, the capillary forces become more important, $\mathscr{C}$ decreases and breakup occurs at progressively shorter liquid bridge lengths. For large capillary numbers and $O(1)$ viscosity ratios, very long threads are obtained which do not fragment as long as the threads are being pulled. Such long, thin, asymmetrical filaments can be obtained in a flow situation where interfacial tension plays a minor role and the outer bath fluid is at least as viscous as the liquid bridge fluid. Additional computations show that long, thin, symmetrical filaments are obtained for high capillary number deformations of liquid bridges when the inner fluid is much more viscous than the outer fluid ($\lambda\gg 1$). In this limit the relative insignificance of viscous interfacial stresses arising from mo-

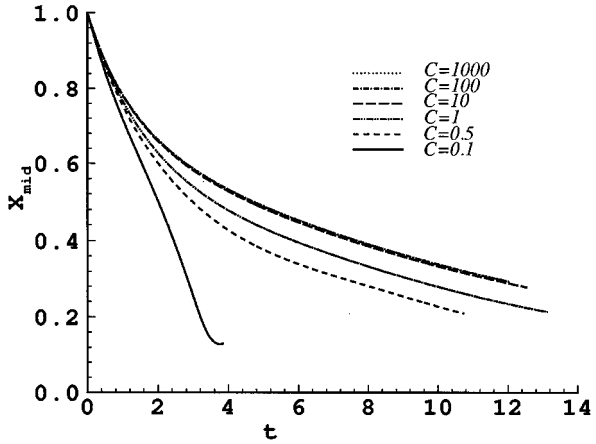

FIG. 16. The effect of $\mathscr{C}$ on the evolution of the liquid bridge mid-point radius; $\lambda=1$, $\Lambda_0=1$, $\mathscr{B}=0$. The curves for $\mathscr{C}=100$ and $\mathscr{C}=1000$ nearly superpose.

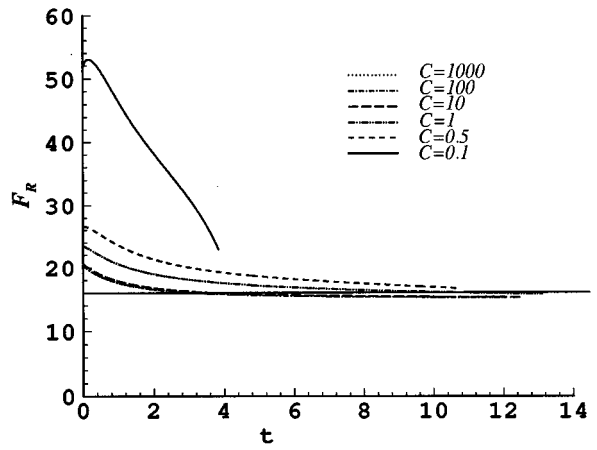

FIG. 17. The effect of $\mathscr{C}$ on the evolution of the applied force on the right end plate; $\lambda=1$, $\Lambda_0=1$, $\mathscr{B}=0$. The curves for $\mathscr{C}=100$ and $\mathscr{C}=1000$ nearly superpose. The horizontal line is the dimensionless drag force on an isolated disk translating in a quiescent fluid (Refs. 38 and 39).

tion of the outer fluid means that the liquid filament retains its fore-aft symmetry at all times. This ability to draw long liquid filaments at high $\mathscr{C}$ contributes to the viability of such configurations for use in measuring extensional viscosities of viscous fluids at large strains.

For these simulations we report in Figs. 16 and 17 the evolution of the interface mid-point radius and the dimensionless applied force $\mathscr{F}_R$ on the right end plate. We observe that the dynamics no longer change for $\mathscr{C}>10$ and the applied force increases as the capillary number decreases by an amount that scales with $\pi/\mathscr{C}$, which is again consistent with equation (14). Furthermore, the force evolves, at least for $\mathscr{C}>0.5$, to a constant value.

Since $\lambda=1$ in the above simulations, the motion of the end plate is similar, at least for large extensions, to the broadside translation of a circular disk in an unbounded, homogeneous, otherwise quiescent fluid. Ray[38] and Gupta[39] determined the dimensionless value of the drag force on the disk, $\mathscr{F}_D=16$, for the broadside disk translation and this result is shown as the solid horizontal line in Fig. 17. The curves for large $\mathscr{C}$ asymptote to $F_R/\mu_1 U R_0 \approx 15.2$, which is slightly below the theoretical result. This difference may be rationalized by realizing that, even for these large values of $\mathscr{C}$, interfacial tension is not identically zero. Therefore, there is a slightly greater pressure within the bridge fluid relative to the outside fluid because of the large interface curvatures. The result is a reduction in the drag force on the plate compared to the case where the interfacial tension vanishes ($\mathscr{C}=\infty$).

E. Effect of initial aspect ratio

Finally, we briefly summarize numerical results on the effects of the initial aspect ratio Λ_0 on the dynamics of the liquid bridge geometry. In Fig. 18 interface shapes are shown for $\mathscr{C}=1$, $\lambda=1$ and $\Lambda_0=0.5,0.75,1,3$, which are all stable static configurations. As the initial aspect ratio increases to $\Lambda_0 \approx 1$, the final length of the fluid column (prior to the numerical calculations indicating thread breakup) also increases due, primarily, to the greater amount of bridge fluid present. However, for $\Lambda_0=3$, thread fragmentation occurs for a final extended bridge length which is shorter than for the case $\Lambda_0=1$. The latter observation can be rationalized by noting from (14) that the viscous effects scale as Λ^{-2} implying that for values of $\Lambda_0>1$ interfacial tension forces become dominant at earlier times.

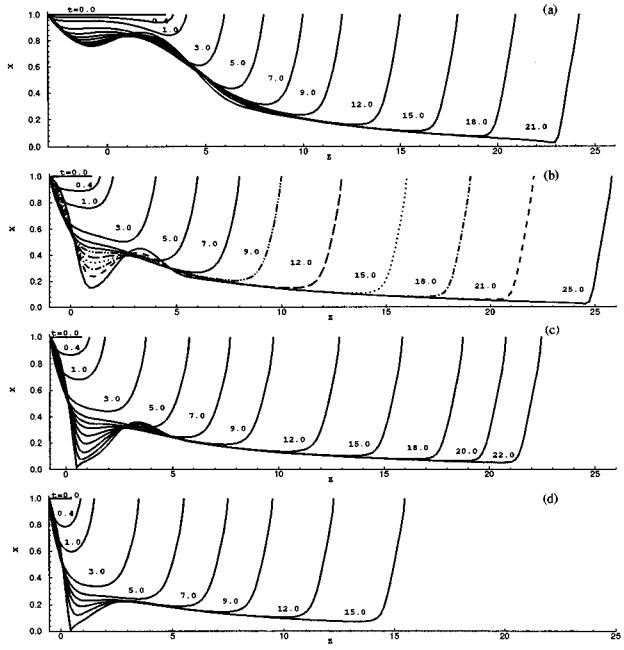

FIG. 18. The effect of Λ_0 on the evolution of the fluid interface; $\mathscr{C}=1$, $\lambda=1$, $\mathscr{B}=0$. (a) $\Lambda_0=3$, (b) $\Lambda_0=1$, (c) $\Lambda_0=0.75$, (d) $\Lambda_0=0.5$.

The results shown in Fig. 19 for the force required to translate the right end plate at unit speed illustrate that bridges with smaller aspect ratios require substantially larger forces to elongate, as expected for a flow with lubrication-like characteristics. Furthermore the viscous contribution to the force at early times varies approximately as Λ^{-2} and at long times (i.e., larger aspect ratios) the total force ap-

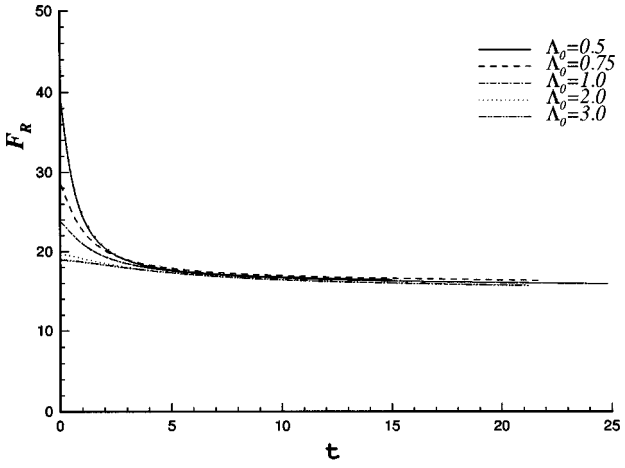

FIG. 19. The effect of Λ_0 on the evolution of the applied force on the right end plate; $\mathscr{C}=1$, $\lambda=1$, $\mathscr{B}=0$.

proaches the approximate dimensionless value of $\mathscr{T}_R = 16$, which is characteristic of an isolated translating disk.

V. CONCLUSIONS

We have presented a study of the statics and dynamics of deforming Newtonian liquid bridges. In particular, we first investigated the static shapes of liquid bridges for the experimentally realizable conditions of fixed bridge volume. The boundary integral method was then applied in order to explore the dynamics at low Reynolds numbers of viscous fluid columns undergoing steady extensional stretching. The simulations were continued almost to breakup, and yield both the evolution of the total force on the end plates and the shape of the distorting bridge as a function of the capillary number, viscosity ratio and initial aspect ratio. Order-of-magnitude estimates for the velocity along the fluid-fluid interface and for the applied force on the end plates provide useful guides for predicting some of the features of stretching flows given values of $\mathscr{C}$, λ and Λ.

Recent work by Eggers[40] has focused on the later stages of breakup of axisymmetric fluid filaments shown in many figures of the present work. In the analysis of Eggers the effects of surface tension, viscous stresses and inertia are all considered to be important and a universal similarity solution independent of the length and time scales imposed by the geometric configuration of the apparatus is developed. The numerical results that we have presented here are for viscous flows for which inertial effects are neglected and do not capture the fine scale details of the breakup process. For a given set of parameters, the numerical simulations indicate the regions where breakup is to occur as well as the approximate time to breakup from an initial configuration.

The dynamical simulations presented in this work can also be used to better understand liquid bridge stretching experiments that are being performed to estimate extensional viscosities of Newtonian and non-Newtonian fluids.[3,30] An important difference between the present calculations and these experiments is in the form of the imposed kinematics at the end plate. An ideal homogeneous uniaxial elongation requires that the sample aspect ratio increase as $\Lambda(t) = \Lambda_0 \exp(\dot{\epsilon} t)$ where $\dot{\epsilon}$ is the imposed extension rate. It is straightforward to implement such boundary data in the present numerical formulation provided that the bridge fluid is sufficiently viscous to ensure inertial accelerations are negligible. We will report on these calculations at a later date, however it is clear from the simulations in the present work that the non-homogeneous flow induced by the rigid end plates will result in non-cylindrical deformations of liquid columns for any values of $\mathscr{C}$, λ or Λ chosen in the experiments. One possible solution to this may be to incorporate flexible end plates which deform radially at a prescribed rate.[4]

ACKNOWLEDGMENTS

We gratefully acknowledge financial support from NASA (grant to GHM), the Petroleum Research Fund (Grant No. 28690-AC9 to HAS) and NSF (Grant No. CTS-8957043 to HAS). Also, we thank Dr. Stephen Spiegelberg for helpful discussions concerning experimental studies of liquid bridges.

[1] A. F. G. Dixon, P. C. Croghan, and R. P. Gowing, ''The mechanism by which aphids adhere to smooth surfaces,'' J. Exp. Biol. **152**, 243 (1990).
[2] G. Hanna and W. J. P. Barnes, ''Adhesion and detachment of the toe pads of tree frogs,'' J. Exp. Biol. **155**, 103 (1991).
[3] T. Sridhar, V. Tirtaatmadja, D. A. Nguyen, and R. K. Gupta, ''Measurement of extensional viscosity of polymer solutions,'' J. Non-Newt. Fluid Mech. **40**, 271 (1991).
[4] S. Berg, R. Kröger, and H. J. Rath, ''Measurement of extensional viscosity by stretching large liquid bridges in microgravity,'' J. Non-Newt. Fluid Mech. **55**, 307 (1994).
[5] R. B. Bird, C. F. Curtiss, R. C. Armstrong, and O. Hassager, *Dynamics of Polymeric Liquids*, 2nd ed. (Wiley, New York, 1987), Vol. I.
[6] C. Macosko, *Rheology: Principles, Measurements and Applications* (VCH, New York, 1993).
[7] F. T. Trouton, ''On the coefficient of viscous traction and its relation to that of viscosity,'' Proc. R. Soc. London Ser. A **77**, 426 (1906).
[8] J. A. F. Plateau, ''Experimental and theoretical researches on the figures of equilibrium of a liquid mass...,'' translated in Annual Reports of the Smithsonian Institution (1863-1866).
[9] M. A. Erle, R. D. Gillette, and D. C. Dyson ''Stability of interfaces of revolution with constant surface tension—The case of the catenoid,'' Chem. Eng. J. **1**, 97 (1970).
[10] R. D. Gillette and D. C. Dyson, ''Stability of fluid interfaces of revolution between equal solid circular plates,'' Chem. Eng. J. **2**, 44 (1971).
[11] S. R. Coriell, S. C. Hardy, and M. R. Cordes, ''Stability of liquid zones,'' J. Colloid Interface Sci. **60**, 126 (1977).
[12] N. A. Bezdenejnykh and J. Meseguer, ''Stability limits of minimum volume and breaking of axisymmetric liquid bridges between unequal disks,'' Micrograv. Sci. Technol. **IV/4**, 235 (1994).
[13] L. A. Slobozhanin and J. M. Perales, ''Stability of liquid bridges between equal disks in an axial gravity field,'' Phys. Fluids A **5**, 1305 (1993).
[14] A. Laverón-Simavilla and J. M. Perales, ''Equilibrium shapes of nonaxisymmetric liquid bridges of arbitrary volume in gravitational fields and their potential energy,'' Phys. Fluids **7**, 1204 (1995).
[15] D. Rivas and J. Meseguer, ''One-dimensional self-similar solution of the dynamics of axisymmetric slender liquid bridges,'' J. Fluid Mech. **138**, 417 (1984).
[16] A. Borkar and J. Tsamopoulos, ''Boundary-layer analysis of the dynamics of axisymmetrical capillary bridges,'' Phys. Fluids A **3**, 2866 (1991).
[17] J. Meseguer and A. Sanz, ''Numerical and experimental study of the dynamics of axisymmetric slender liquid bridges,'' J. Fluid Mech. **153**, 83 (1985).
[18] J. Meseguer and M. Perales, ''Non-steady phenomena in the vibration of viscous, cylindrical, long liquid bridges,'' Micrograv. Sci. Technol. **V/2**, 69 (1992).
[19] A. Sanz, ''The influence of the outer bath in the dynamics of axisymmetric liquid bridges,'' J. Fluid Mech. **156**, 101 (1985).
[20] J. A. Nicolas, ''Hydrodynamic stability of high-viscosity cylindrical liquid bridges,'' Phys. Fluids A **4**, 1620 (1992).
[21] J. Tsamopoulos, T.-Y. Chen, and A. Borkar, ''Viscous oscillations of capillary bridges,'' J. Fluid Mech. **235**, 579 (1992).
[22] T.-Y. Chen and J. Tsamopoulos, ''Nonlinear dynamics of capillary bridges: Theory,'' J. Fluid Mech. **255**, 373 (1993).
[23] I. Martinez and A. Croll, ''Liquid bridges and floating zones,'' *Fluid Physics, Lecture Notes of Summer Schools*, edited by M. G. Velarde and C. I. Christov (World Scientific, Singapore, 1994).
[24] B. J. Lowry and P. H. Steen, ''Stabilization of an axisymmetric liquid bridge by viscous flow,'' Int. J. Multiphase Flow **20**, 439 (1994).
[25] H. A. Dijkstra, ''On the shear stabilization of capillary break-up of finite liquid bridges,'' Micrograv. Sci. Technol. **VI/1**, 13 (1993).
[26] A. M. J. Davis and A. L. Frenkel, ''Cylindrical liquid bridges squeezed between parallel plates: Exact Stokes flow solutions and hydrodynamic forces,'' Phys. Fluids A **4**, 1105 (1992).
[27] J. E. Matta and R. P. Tytus, ''Liquid stretching using a falling cylinder,'' J. Non-Newt. Fluid Mech. **35**, 215 (1990).
[28] R. Kröger, S. Berg, A. Delgado, and H. J. Rath, ''Stretching behavior of large polymeric and Newtonian liquid bridges in Plateau simulation,'' J. Non-Newt. Fluid Mech. **45**, 385 (1992).

[29]A. Delgado, ''Non-Newtonian effects under microgravity conditions,'' Micrograv. Sci. Technol. **4**, 12 (1991).
[30]S. H. Spiegelberg, S. Gaudet, and G. H. McKinley, ''Extensional deformation of non-Newtonian materials: Liquid bridge studies,'' *2nd Microgravity Fluid Physics Conference*, Cleveland, OH, 1994, Vol. CP-3276 (US Govt. Printing Office 1994-553-454), p. 311.
[31]R. W. G. Shipman, M. M. Denn, and R. Keunings, ''Mechanics of the falling plate extensional rheometer,'' J. Non-Newt. Fluid Mech. **40**, 281 (1991).
[32]A. Sanz and I. Martinez, ''Minimum volume for a liquid bridge between equal disks,'' J. Colloid Interface Sci. **93**, 235 (1983).
[33]J. M. Rallison and A. Acrivos, ''A numerical study of the deformation and burst of a viscous drop in an extensional flow,'' J. Fluid Mech. **89**, 191 (1978).
[34]C. Pozrikidis, *Boundary Integral and Singularity Methods for Linearized Viscous Flow* (Cambridge University Press, Cambridge, 1992).
[35]J. Tanzosh, M. Manga, and H. A. Stone, ''Boundary integral methods for viscous free-boundary problems: Deformation of single and multiple fluid-fluid interfaces,'' *Proceedings of Boundary Element Technologies VII*, edited by C. A. Brebbia and M. S. Ingber (Computational Mechanics Publications, 1992), p. 19.
[36]S. H. Lee and L. G. Leal, ''The motion of a sphere in the presence of a deformable interface,'' J. Colloid Interface. Sci. **87**, 81 (1982).
[37]H. A. Stone and L. G. Leal, ''Relaxation and breakup of an initially extended drop in an otherwise quiescent fluid,'' J. Fluid Mech. **198**, 399 (1989).
[38]M. Ray, ''Application of Bessel functions to the solution of problems of motion of a circular disk in viscous liquid,'' Philos. Mag. **21**, 546 (1936).
[39]S. C. Gupta, ''Slow broad side motion of a flat plate in a viscous fluid,'' Z. Angew Math. Phys. **8**, 257 (1957).
[40]J. Eggers, ''Theory of drop formation,'' Phys. Fluids **7**, 941 (1995).